The energy level structure of low-dimensional multi-electron quantum dots

Tokuei Sako, [a] * Josef Paldus [b] † and Geerd H. F. Diercksen [c] ‡

[a]Laboratory of Physics, College of Science and Technology, Nihon University, 7-24-1 Narashinodai, Funabashi, 274-8501 Chiba, Japan

[b]Department of Applied Mathematics, University of Waterloo, Waterloo, Ontario N2L 3G1, Canada

[c]Max-Planck-Institut für Astrophysik, Karl-Schwarzschild-Strasse 1, D-85741 Garching, Germany

A unified characterization of the energy-level structure of quasi-one-dimensional quantum dots is presented based on accurate computational results for the eigenenergies and wave functions, as obtained in previous studies for the case of two and three electrons, and in the present study also for four electrons. In each case the quantum chemical full configuration interaction method is adopted employing Cartesian anisotropic Gaussian basis sets. The energy-level structure is shown to be strongly dependent on the confinement strength ω and can be exemplified by the three qualitatively distinct regimes for large, medium, and small confinement strengths. To characterize the energy-level structure in the large or medium ω and the small ω regimes, the polyad quantum number, as well as its *extended* version, the *extended* polyad quantum number have been introduced. The degeneracy of energy levels for different spin states in the small ω regime is shown to be caused by the *potential walls* of the electron-electron interaction potential within the internal space. A systematic way of obtaining the degeneracy pattern of the energy levels in the small ω regime is also presented. Finally, qualitative differences between the energy-level structure of quasi-one-dimensional and quasi-two-dimensional quantum dots in the small ω regime are briefly discussed by referring to the different structure of their internal spaces.

1. INTRODUCTION

Confined quantum systems of a finite number of electrons bound in a fabricated nanoscale potential, typically of the order of $1 \sim 100$ nm, are referred to as quantum dots or

*email: sako@phys.ge.cst.nihon-u.ac.jp, homepage: www.phys.ge.cst.nihon-u.ac.jp/~sako/, TS has been supported in part by the Grants-in-Aid for Scientific Research (No.20750018) from the Ministry of Education, Science, Sports and Culture.

†email: paldus@scienide2.uwaterloo.ca, JP thanks the Alexander von Humboldt Foundation for his fellowship.

‡email: ghd@mpa-garching.mpg.de, homepage: www.mpa-garching.mpg.de/mol_physics/index.shtml

artificial atoms [1–4] since they have a discrete energy-level structure following Hund's rules [5,6]. The properties quantum dots can be controlled by changing the size and/or the shape of the fabricated potential [7–9]. Quantum dots are known to show features in their energy-level structure and their optical properties qualitatively different from atoms [10,11]. The differences between quantum dots and atoms are due to the harmonic nature of the confining potential of quantum dots as compared to the Coulomb potential of atoms [4,12,13] as well as to the larger size and the lower dimensionality of quantum dots [14,15].

Computational techniques based on the quantum chemical molecular orbital theory make it possible to calculate the properties of not only the ground state but also of the low-lying excited states of multi-electron quantum dots for a specific value of the strength of confinement. As the calculated results vary strongly for different strengths of confinement due to a strong variation of the relative importance of the electron-electron interaction with respect to the change of the strength of confinement [4,12,16–18], it is necessary to develop a unified method for interpreting the complicated energy-level structure of quantum dots for the whole range of the strength of confinement.

In previous studies of this series it was found that the *polyad quantum number* [19] defined by the total number of nodes in the leading configuration of the configuration interaction (CI) wave function is approximately conserved for harmonic-oscillator quantum dots. The polyad quantum number and its extension can be used to characterize the energy spectra of quasi-one-dimensional quantum dots of two and three electrons for the whole range of the strength of confinement [20,21]. Energy levels belonging to different polyad quantum numbers and having different spin multiplicities are converging to nearly degenerate levels as the strength of confinement becomes smaller. This convergence is caused by increasingly stronger potential walls of the electron-electron interaction potentials that modify significantly the nodal pattern of the wave function of lower spin states while affecting little the wave function of the highest spin states [20,21].

In the present contribution the interpretation of the energy-level structure of quasi-one-dimensional quantum dots of two and three electrons is reviewed in detail by examining the polyad structure of the energy levels and the symmetry of the spatial part of the CI wave functions due to the Pauli principle. The interpretation based on the polyad quantum number is applied to the four electron case and is shown to be applicable to general multi-electron cases. The qualitative differences in the energy-level structure between quasi-one-dimensional and quasi-*two*-dimensional quantum dots are briefly discussed by referring to their differences in the structure of the *internal space*.

2. COMPUTATIONAL METHODOLOGY

2.1. Theoretical model

The Hamiltonian operator for a confined quantum system is written as

$$\mathcal{H} = \sum_{i=1}^{N} \left[-\tfrac{1}{2}\nabla_i^2 \right] + \sum_{i=1}^{N} w(\mathbf{r}_i) + \sum_{i>j}^{N} \frac{1}{|\mathbf{r}_i - \mathbf{r}_j|}, \tag{1}$$

where N denotes the number of electrons and w denotes the one-electron confining potential [16,22]. In the present study the one-electron confining potential w for the quasi-

one-dimensional quantum dots is given by

$$w_{q1D}(\boldsymbol{r}) = \tfrac{1}{2}\omega_{xy}^2\left(x^2+y^2\right) - D\exp\left[-\frac{\omega_z^2}{2D}z^2\right], \tag{2}$$

and for the quasi-two-dimensional quantum dots it is given by

$$w_{q2D}(\boldsymbol{r}) = -D\exp\left[-\frac{\omega_{xy}^2}{2D}(x^2+y^2)\right] + \tfrac{1}{2}\omega_z^2 z^2. \tag{3}$$

The potentials of Eqs. (2) and (3) represent the sum of harmonic-oscillator and attractive Gaussian potentials. For a sufficiently large value of ω_{xy} in Eq. (2) the electrons bound by this potential are strongly compressed along the x and y directions and have degrees of freedom only along the z direction. Therefore, the one-electron potential w_{q1D} of Eq. (2) represents the confining potential of quasi-one-dimensional quantum dots with a shape like a 'pipe'. Similarly, for a sufficiently large value of ω_z in Eq. (3) the electrons in this potential are strongly compressed along the z direction and have degrees of freedom only in the xy plane. Therefore, the potential w_{q2D} of Eq. (3) represents the confining potential of quasi-two-dimensional quantum dots having a shape like a 'disk'. A Gaussian potential has been chosen as the confining potential, among others, because it is approximated in the low energy region by a harmonic-oscillator potential typically used for modeling semiconductor quantum dots [13,12,4]. The value of the parameters ω_{xy} and ω_z is set to 20 a.u. for all results presented in this contribution and this is not indicated explicitly hereafter.

The *anharmonicity* of the confining potential can be controlled by changing the 'depth' of the Gaussian potential D with respect to ω_z and ω_{xy}, respectively. The parameters ω_z and ω_{xy} represent the frequency of the harmonic-oscillator potential characterizing the strength of confinement of the Gaussian potential. They are obtained by a quadratic approximation to the Gaussian potential in Eqs. (2) and (3), respectively. When D is much larger than the harmonic frequency the Gaussian potential closely follows the harmonic-oscillator potential in the low energy region. This indicates that the anharmonicity is small. On the other hand, when D is only slightly larger than the harmonic frequency the Gaussian potential deviates strongly from the harmonic-oscillator potential even in the low energy region. This indicates that the anharmonicity is large. The extent of anharmonicity may be specified by the parameter α [20] which is defined for the quasi-one-dimensional quantum dots by

$$\alpha_{q1D} = \omega_z/D, \tag{4}$$

and for the quasi-two-dimensional quantum dots by

$$\alpha_{q2D} = \omega_{xy}/D. \tag{5}$$

Introducing anharmonicity is important for simulating realistic confining potentials [23, 24].

The total energies and wavefunctions of the Hamiltonian (1) have been calculated as the eigenvalues and eigenvectors of a CI matrix. Full CI has been used for all calculations of quasi-one-dimensional quantum dots and for quasi-two-dimensional quantum dots with

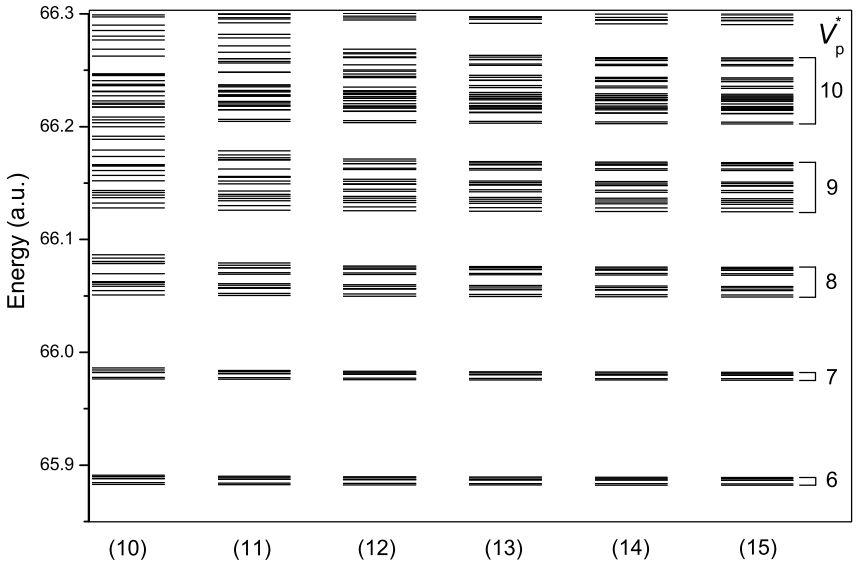

Figure 1. (Color online) Energy spectrum of the low-lying states of four electrons confined in a quasi-one-dimensional Gaussian potential with $(D, \omega_z, \omega_{xy}) = (4.0,\ 0.1,\ 20.0)$ for different-size basis sets. Energy levels of different spin multiplicities are indicated by different colors (See the caption to Fig. 2). The number in the round brackets specifies the total number of basis functions and the parameter v_p^* specifies the *extended* polyad quantum number (See the text for details).

$N = 2$ while multi-reference CI has been used for quasi-two-dimensional quantum dots with $N = 3$ and 4. The results are presented in atomic units. They can be scaled by the effective Bohr radius of 9.79 nm and the effective Hartree energy of 11.9 meV for GaAs semiconductor quantum dots [25,26].

2.2. Basis sets employed

In order to properly describe the wave function of electrons confined in a strongly anisotropic potential given by Eqs. (2) and (3) a set of properly chosen Cartesian *anisotropic* Gaussian-type orbitals (c-aniGTO) [16,17,22] have been adopted as basis set spanning the one-electron orbital space. The general form of an unnormalized c-aniGTO function placed at (b_x, b_y, b_z) is given by

$$\chi_{ani}^{\vec{a},\vec{\zeta}}(\vec{r};\vec{b}) = x_{b_x}^{a_x} y_{b_y}^{a_y} z_{b_z}^{a_z} exp\left(-\zeta_x x_{b_x}^2 - \zeta_y y_{b_y}^2 - \zeta_z z_{b_z}^2\right), \tag{6}$$

where the shorthand notation x_{b_x} is used for $(x - b_x)$, etc. Unlike standard Gaussian-type orbitals the c-aniGTO functions can be easily fitted to properly describe the wavefunction of electrons in an anisotropic confining potential by adjusting the three exponents ζ_x, ζ_y and ζ_z independently. In principle, a Gaussian basis set of floating standard Gaussian functions could be used for this purpose but this would require an extremely large number of functions at different points in space in order to properly describe the distribution of the electrons. A c-aniGTO basis set can be transformed into a set of eigenfunctions of the

corresponding three-dimensional anisotropic harmonic oscillator [17]. Consequently, such a basis set is also useful in high-accuracy calculations of eigenvalues and eigenfunctions of atoms in strong magnetic fields [27–30] and of semiconductor quantum dots [31,32].

In the present study a c-aniGTO basis set has been placed at the center of the confining potential, i.e. at the origin of the Cartesian coordinate system. The orbital exponents for the harmonic-oscillator potential in the Eqs. (2) and (3) have been chosen as one half of the strength of the confinement, ω_{xy} and ω_z, respectively, while the exponents for the Gaussian potentials have been determined in the same way as described in a previous study [19]. Since the strength of the confinement for the harmonic-oscillator potential is much larger than that for the Gaussian potential, only functions *without* nodes along the direction of the harmonic-oscillator potential have been selected and used in the basis sets [18–20]. The size of the basis set required for calculating a reliable energy spectrum has been determined by following the convergence of the energies while stepwise increasing its size. The pattern of convergence for the case of four electrons with $(D, \omega_z) = (4.0,\ 0.1)$ is displayed in Fig. 1. The number of basis functions, indicated by the number enclosed in parentheses, was increased stepwise by adding in each step a new function with an additional node. The energy spectrum calculated with 10 basis functions displayed on the left-hand side of Fig. 1 differs for $E \geq 66.1$ significantly from the spectrum calculated by using the next larger basis with 11 functions, indicating the inadequacy of the former basis. It is noted that the basis set with 10 functions already includes a function with the angular momentum quantum number $l = 9$. Thus, a basis set with very high angular momentum functions is clearly required for a reliable description of strongly anisotropic quantum dots. As shown in Fig. 1 the energy-level structure becomes stabilized as the number of basis functions increases. The maximum deviation between the energy levels up to the fifth band with $v_p^* = 10$ calculated by using the basis sets with 14 and 15 functions, respectively, is smaller than $5.7{\times}10^{-4}$. In the calculations involving four electrons that are presented in this study a basis set consisting of 16 functions has been used. The convergence characteristic for the case of two electrons was given already in Ref. [20] and for the case of three electrons in Ref. [21].

3. QUASI-ONE-DIMENSIONAL QUANTUM DOTS

3.1. Energy spectrum: general outlook

The confinement strength ω_z of quasi-one-dimensional quantum dots can be classified according to the relative size of the one-electron energy E_1 and the two-electron energy E_2. The one-electron energy of the one-dimensional harmonic oscillator is given by $\omega_z(n + \frac{1}{2})$, with n denoting the harmonic-oscillator quantum number. Thus, it scales linearly with ω_z, i.e., $E_1 \sim \omega_z$. The two-electron energy can be estimated by considering l_z of the system along the z direction [33]. The characteristic length is related to ω_z by $l_z \sim 1/\sqrt{\omega_z}$ since the probability distribution of the one-dimensional harmonic-oscillator ground state with the frequency ω_z is proportional to $\exp\left[-\frac{1}{2}\omega_z z^2\right]$. Thus, the two-electron energy which is related to l_z by $E_2 \sim 1/l_z$ is scaled by ω_z as $E_2 \sim \sqrt{\omega_z}$. Consequently, the one-electron energy E_1 dominates the total energy for $w_z \gg 1.0$ (large ω_z). Its contribution to the total energy becomes similar to that of E_2 for $w_z \sim 1.0$ (medium ω_z), while the two-electron energy E_2 dominates the total energy for $w_z \ll 1.0$ (small ω_z) [21].

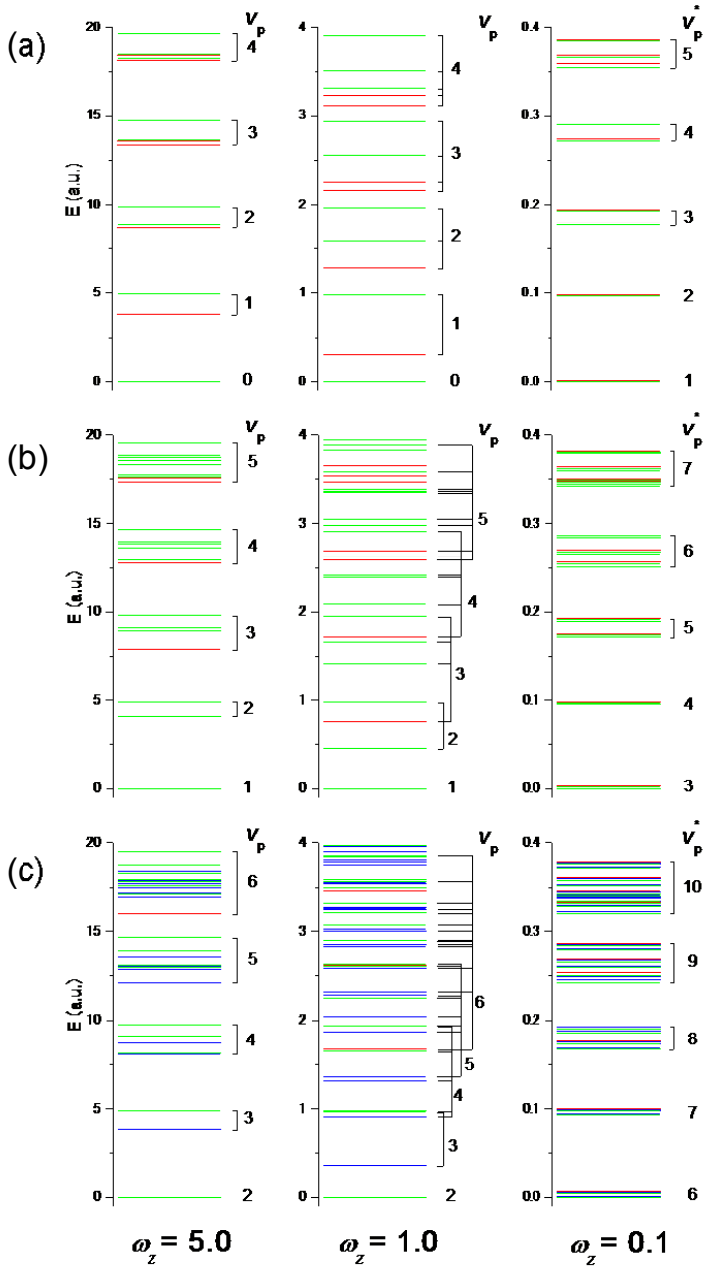

Figure 2. (Color online) Energy spectrum of N electrons confined by a quasi-one-dimensional Gaussian potential with different strength of confinement ω_z for $N = 2$ (a), 3 (b), and 4 (c), respectively, represented as relative energies from the ground state. The anharmonicity parameter α of the Gaussian potential is 0.025 in all cases. Energy levels for different spin multiplicities are indicated by different colors: in (a), the singlets and triplets are colored by green and red, respectively, in (b), the doublets and quartets by green and red, respectively, and in (c), the singlets, triplets, and quintets by green, blue, and red, respectively.

The energy spectra of N electrons confined by the quasi-one-dimensional Gaussian potentials with $(D, \omega_z) = (200.0, 5.0)$, (40.0, 1.0), and (4.0, 0.1) are displayed in Figs. 2 (a), (b), and (c) for $N = 2$, 3, and 4, respectively. The ω_z values of 5.0, 1.0, and 0.1, correspond to the three regimes of confinement strength defined above, namely, large, medium, and small. Energy levels with different spin multiplicities are displayed in different colors: for $N = 2$ (Fig. 2(a)) the singlets and triplets are displayed in green and red, for $N = 3$ (Fig. 2(b)) the doublets and quartets are displayed also in green and red, and for $N = 4$ (Fig. 2(c)) the singlets, triplets, and quintets are displayed in green, blue, and red. The anharmonicity parameter α is equal to 0.025 in all cases. This corresponds to an approximately harmonic Gaussian potential. The vertical axis of each of the three energy diagrams for different confinement strengths is scaled by ω_z so that the energy of the ground state and the excitation energy of 4 quanta of ω_z appear on the vertical axis at the same level [20,21]. Therefore in the *absence* of electron-electron interaction all three energy spectra would look identical in this representation.

As shown in Fig. 2 the energy level structure changes dramatically for the three regimes of confinement strength ω_z: The energy spectrum for the large confinement regime displayed on the left-hand side of Fig. 2 shows a harmonic band structure with a band gap close to ω_z. The energy spectrum for the medium confinement regime displayed in the middle of the figure shows a broader distribution of energy levels. On the other hand, the energy spectrum in the small confinement regime displayed on the right-hand side of the figure shows again a harmonic band structure with a band gap close to to ω_z. But this energy spectrum is characterized by a different number of levels with different spin multiplicities in each band as compared to the case of the large confinement regime. These observations apply to all cases of $N = 2$, 3, and 4. In the next section the changes in the energy spectrum due to different confinement strength are interpreted by exploiting the concept of the *polyad quantum number*.

3.2. Polyad structure

The polyad quantum number is defined as the sum of the number of nodes of the one-electron orbitals in the leading configuration of the CI wave function [19]. The name *polyad* originates from molecular vibrational spectroscopy, where such a quantum number is used to characterize a group of vibrational states for which the individual states cannot be assigned by a set of normal-mode quantum numbers due to a mixing of different vibrational modes [19]. In the present case of quasi-one-dimensional quantum dots the polyad quantum number can be defined as the sum of the one-dimensional harmonic-oscillator quantum numbers for all electrons.

The harmonic-band structure of the energy spectrum of quasi-one-dimensional quantum dots for the large ω_z regime can be understood by exploiting the polyad quantum number. In the large ω_z regime the one-electron energy E_1 dominates the total energy and the electron-electron interaction represents only a small perturbation. Therefore, in a zeroth-order approximation, the Hamiltonian of the system can be written as a sum of N harmonic-oscillator Hamiltonians

$$\mathcal{H}_0 = \sum_{i=1}^{N} \left[-\tfrac{1}{2} \left(\frac{\partial}{\partial z_i} \right)^2 + \tfrac{1}{2} \omega_z^2 z_i^2 \right], \tag{7}$$

where the x and y degrees of freedom are ignored and the Gaussian potential along the z direction is approximated by a harmonic oscillator with the frequency ω_z. The energy of the Hamiltonian (7) can then be expressed in terms of the polyad quantum number, denoted hereafter by v_p, as follows

$$E_{\vec{n}} = \omega_z \left[v_p + \tfrac{N}{2} \right], \tag{8}$$

with

$$v_p = \sum_{i=1}^{N} n_i, \tag{9}$$

where $\vec{n}$ =(n_1, n_2, ..., n_N) represents the harmonic-oscillator quantum numbers for the electron 1, 2, .., N, respectively. Equation (8) shows that energy levels having the same value of v_p are degenerate and that those having different values of v_p are separated by a multiple of ω_z. This explains why the energy-level structure for the large ω_z regime has a harmonic-band structure with a spacing of ω_z as observed on the left-hand side of Fig. 2.

It is noted, however, that not all possible combinations of $(n_1, n_2, ..., n_N)$ can be realized as quantum states. Because of the Pauli principle the total wave function involving both the spatial and spin parts must be antisymmetric with respect to the interchange of any two electron coordinates. In order to construct electronic quantum states for the Hamiltonian (7) satisfying the Pauli principle it is convenient to impose a restriction on the set $(n_1, n_2, ..., n_N)$ by requiring that $n_1 \leq n_2 \leq ... \leq n_N$, where the same value of n_i cannot appear more than twice. In order to satisfy the Pauli principle a chosen $\vec{n}$, representing a spatial orbital configuration should be coupled with the appropriate spin functions. In the case of two electrons the configuration (n_a, n_b) $(n_a \neq n_b)$ can be coupled to the singlet and the triplet spin functions. On the other hand the configuration (n_a, n_a) can be coupled only to the singlet spin function since the latter configuration is symmetric with respect to the interchange of the electron coordinates 1 and 2 and thus must be coupled with an antisymmetric spin function. For example in case of the polyad manifold $v_p = 2$ there are two configurations, (0,2) and (1,1). The (0,2) configuration is coupled both to the singlet and triplet spin functions while the (1,1) configuration is coupled only to the singlet spin function resulting in a total of three electronic states. Similar arguments can be applied to all v_p manifolds and it can be shown that for the two-electron case the number of levels in each v_p manifold amounts to $(v_p + 1)$ as may be seen in Fig. 2(a).

The situation becomes slightly complicated for systems with more than two electrons due to the *spin degeneracy*. In the case of three electrons, for example, one can construct doublet ($S = \frac{1}{2}$) and quartet ($S = \frac{3}{2}$) spin states denoted by $\left|\frac{1}{2}, M\right\rangle$ ($M = -\frac{1}{2}, \frac{1}{2}$) and $\left|\frac{3}{2}, M\right\rangle$ ($M = -\frac{3}{2}, -\frac{1}{2}, \frac{1}{2}, \frac{3}{2}$), respectively. States with different magnetic quantum numbers M are degenerate in the absence of spin-dependent interactions, such as spin-orbit interaction. It should be noted, however, that for a given $|S, M\rangle$ state there is only one quartet state while there are *two* doublet states. These two doublet spin states are linearly independent and, in general, have different energies. Therefore three spin states will participate in forming the energy-level structure for three electron quantum dots. The three spin functions with the highest M value, namely, $\left|\frac{3}{2}, \frac{3}{2}\right\rangle$ and $\left|\frac{1}{2}, \frac{1}{2}\right\rangle$ for the quartet and

Table 1
Orbital configuration, number of levels derived from the configuration, and the total number of levels belonging to each v_p manifold for three electrons.

v_p	N_p[1]	config.	n^2
1	1	(1,0,0)	1
2	2	(2,0,0)	1
		(0,1,1)	1
3	4	(3,0,0)	1
		(0,1,2)	3
4	6	(4,0,0)	1
		(0,1,3)	3
		(2,1,1)	1
		(0,2,2)	1
5	9	(5,0,0)	1
		(0,1,4)	3
		(3,1,1)	1
		(0,2,3)	3
		(1,2,2)	1

[1]Number of levels belonging to each v_p manifold.

[2]Number of levels derived by each configuration.

the doublet states, respectively, may be written as $\alpha(1)\alpha(2)\alpha(3)$ for the quartet state, and $\frac{1}{\sqrt{2}}\alpha(1)[\alpha(2)\beta(3)-\beta(2)\alpha(3)]$ and $\frac{1}{\sqrt{6}}[2\beta(1)\alpha(2)\alpha(3)-\alpha(1)\alpha(2)\beta(3)-\alpha(1)\beta(2)\alpha(3)]$ for the two doublet states. In constructing the two doublet spin functions it has been assumed that the first function $\frac{1}{\sqrt{2}}\alpha(1)[\alpha(2)\beta(3)-\beta(2)\alpha(3)]$ (denoted hereafter by $\left|\frac{1}{2},\frac{1}{2}\right\rangle_a$) forms a *two-electron singlet* for the electron pair 2 and 3. The second doublet spin function $\frac{1}{\sqrt{6}}[2\beta(1)\alpha(2)\alpha(3)-\alpha(1)\alpha(2)\beta(3)-\alpha(1)\beta(2)\alpha(3)]$ (denoted hereafter by $\left|\frac{1}{2},\frac{1}{2}\right\rangle_b$) has been obtained by requiring it be orthogonal to $\left|\frac{1}{2},\frac{1}{2}\right\rangle_a$. The spatial orbital configurations for the three electrons have one of the following forms: (n_a, n_b, n_c), (n_a, n_a, n_b), and (n_a, n_b, n_b) with $n_a \neq n_b \neq n_c$. The latter two configurations have a doubly occupied orbital for the electron pairs (1,2) and (2,3). Thus the spin function which forms a two-electron singlet for the electron pairs (1,2) and (2,3) should be coupled with configurations of the type (n_a, n_a, n_b) and (n_a, n_b, n_b) since it has to be antisymmetric with respect to the exchange of the electron pairs (1,2) and (2,3). It is convenient to impose on the orbital configuration $(n_1, n_2, ..., n_N)$ the restriction that the singly occupied orbitals always precede the doubly occupied [34]. With this restriction the latter two three-electron configurations can be represented by the configuration (n_a, n_b, n_b). The three electron ground state has then the configuration (1,0,0) and has to be coupled with the spin function $\left|\frac{1}{2},\frac{1}{2}\right\rangle_a$ giving rise to one level as shown in Fig. 2 (b). In the case of $v_p = 2$ the two configurations (0,1,1) and (2,0,0) are possible. Both of these configurations have to be coupled with the spin function $\left|\frac{1}{2},\frac{1}{2}\right\rangle_a$ giving rise to two levels. In the case of $v_p = 3$ the configuration (0,1,2) with three distinct orbitals will appear in addition to the configuration (3,0,0). The configuration (0,1,2) can be coupled with all three spin functions giving rise to three levels resulting in four levels in total associated with the polyad manifold of $v_p = 3$. A summary of the number of levels and orbital configurations of low-lying polyad manifolds of three electrons has been displayed in Table 1.

The situation becomes more complicated for a system with four electrons but similar arguments as in the three electron case can be applied. The total spin S in the four electron case can take three distinct values, namely, S = 0 (singlet), 1 (triplet), and 2 (quintet). According to the spin branching diagram the degree of degeneracy that is associated with the singlet, triplet and quintet states is 2, 3 and 1, respectively [35]. The ground state of the four electron case has the configuration (0,0,1,1). This configuration belongs to the polyad manifold of $v_p = 2$ and gives rise to one level since it can only be coupled with the singlet spin function consisting of the two-electron singlets for the electron pairs (1,2) and (3,4). The next polyad manifolds of $v_p = 3$ also involves only one configuration, namely (1,2,0,0), which can be coupled with one singlet and one triplet spin function forming a two-electron singlet for the electron pair (1,2) giving rise of a total of two levels as shown in Fig. 2 (c). The same procedure can be applied to the polyad manifold of v_p =4 and 5 giving rise to a total of 5 and 8 levels, respectively. In the case of the polyad manifold of $v_p = 6$ there are five possible configurations: (1,5,0,0), (2,4,0,0), (0,4,1,1), (0,0,3,3), and (0,1,2,3). The first three configurations form a two-electron singlet for the electron pair (3,4) giving rise to one singlet and one triplet level. The fourth configuration forms two-electron singlets for the electron pairs (1,2) and (3,4) giving rise to only one singlet level as in the case of $v_p = 2$ and 3. In the fifth configuration (0,1,2,3) all four orbitals are different and 6 linearly independent spin functions can be coupled with this

Table 2
Orbital configuration, number of levels derived from the configuration, and the total number of levels belonging to each v_p manifold for four electrons.

v_p	N_p[1]	config.	n[2]
2	1	(0,0,1,1)	1
3	2	(1,2,0,0)	2
4	5	(1,3,0,0)	2
		(0,0,2,2)	1
		(0,2,1,1)	2
5	8	(1,4,0,0)	2
		(2,3,0,0)	2
		(0,3,1,1)	2
		(0,1,2,2)	2
6	13	(1,5,0,0)	2
		(2,4,0,0)	2
		(0,4,1,1)	2
		(0,0,3,3)	1
		(0,1,2,3)	6

[1]Number of levels belonging to each v_p manifold.

[2]Number of levels derived from each configuration.

configuration giving rise to 6 levels. Thus, a total of 13 levels is associated with this polyad manifold. The number of levels and orbital configurations for the low-lying polyad manifolds of four electrons are summarized in Table 2. The number of levels calculated for each polyad manifold listed in the table agrees with the results displayed in Fig. 2 (c) for all v_p manifolds.

As the confinement strength ω_z decreases the electron-electron interaction, which represents only a small perturbation for large ω_z, starts to influence the energy spectrum. As a result the splitting of the energy levels belonging to a polyad manifold becomes so large that the energy levels of neighboring polyad manifolds start to overlap as is apparent from Fig. 2 for the medium confinement regime of $\omega_z = 1.0$. When ω_z decreases even further the overlap of the energy levels belonging to different polyad manifolds becomes even larger. Since the polyad quantum number represents an approximately conserved quantity it may be expected that the breakdown of this constant of motion will lead to an irregular energy-level pattern known as quantum chaos. On the other hand, the energy spectra shown in Fig. 2 for the small confinement regime of $\omega_z = 0.1$ show for all cases of $N = 2$, 3, and 4 again a band structure as in the case of the large confinement regime. The reason for the reappearance of such a regular band structure in the energy spectrum for the small confinement regime is examined in detail in the next section.

3.3. Extended polyad structure

The energy spectrum for the small confinement regime ($\omega_z = 0.1$) is displayed on the right hand side of Fig. 2. It shows a band structure similar to that of the strong confinement regime with $\omega_z = 5.0$ characterized by an energy gap close to ω_z. It should be noticed, however, that the energy spectrum for the weak confinement regime differs from that of strong confinement regime by the fact that in the weak confinement regime the energy spectrum consists of groups of nearly degenerate levels having different spin multiplicities. In the case of $N = 2$, 3, and 4 the number of nearly degenerate levels is 2 (singlet and triplet), 3 (two doublets and one quartet), and 6 (two singlets, three triplets, and one quintet), respectively. Therefore, in the weak confinement regime all linearly independent spin states become degenerate. A similar multiplet structure was reported previously for a small number of electrons confined in a large quasi-one-dimensional rectangular potential well [33,36] that may be considered as an indication of the formation of the Wigner lattice [37]. It is also noted that the number of levels belonging to each band of the energy spectrum is different for the small and large ω_z regimes. In the case of $N = 2$, for example, the number of levels belonging to each band, counted from below, is 2, 2, 4, 4, $\cdots$ for $\omega_z = 0.1$, and 1, 2, 3, 4, $\cdots$ for $\omega_z = 5.0$.

In order to explain the band structure for the small confinement regime the nature of the potential energy function in the Hamiltonian has been examined in the *internal space*. Since for quasi-one-dimensional quantum dots the electrons can only move along the z coordinate their x and y dependence is neglected in the analysis. The internal space is defined by a unitary transformation from the independent electron coordinates (z_1, z_2, $\cdots$, z_N) into the correlated electron coordinates (z_α, z_β, $\cdots$). The coordinate z_α represents the totally symmetric *center-of-mass* coordinate $z_\alpha = \frac{1}{\sqrt{N}}(z_1 + z_2 + \cdots + z_N)$ and the remaining correlated electron coordinates z_β, $\cdots$, z_N represent the internal degrees of freedom of the N electrons [20,21]. In the case of two electrons the correlated coordinates

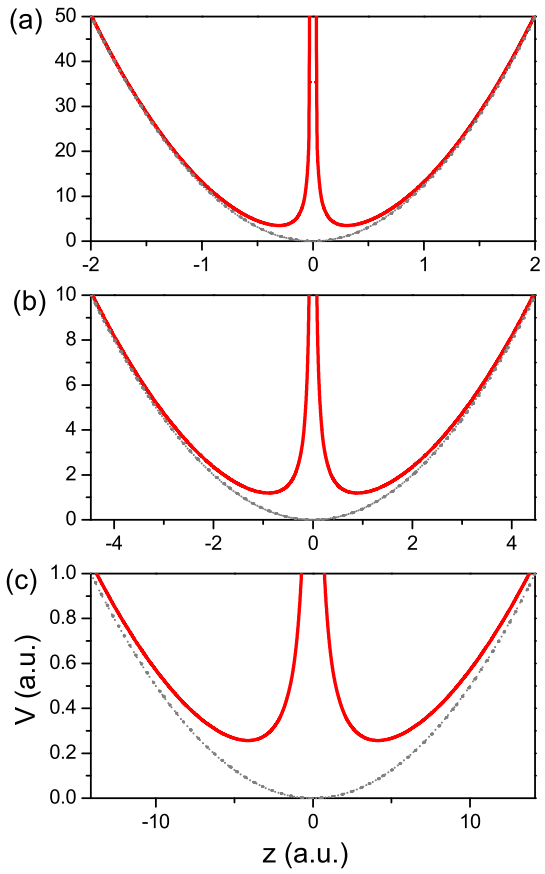

Figure 3. (Color online) One-dimensional plot of the sum of the harmonic-oscillator and of the electron-repulsion potentials V for two electrons as function of the internal coordinate z_a for $\omega_z = 5.0$ (a), 1.0 (b), and 0.1 (c). The solid red line represents the sum of the harmonic-oscillator and the electron repulsion potentials, while the dotted grey line represents only the harmonic-oscillator potential. The maximum potential height V_{max} and the domain of the z_a coordinate displayed are $V_{max} = \omega_z \times 10$ and $|z_a| \leq \sqrt{\frac{20}{\omega_z}}$, respectively, for all cases.

are defined by

$$\begin{aligned} z_s &= \frac{1}{\sqrt{2}}[z_1 + z_2], \\ z_a &= \frac{1}{\sqrt{2}}[z_1 - z_2]. \end{aligned} \tag{10}$$

The symmetric z_s coordinate describes the center-of-mass degree of freedom for the two electrons while the antisymmetric z_a coordinate describes the internal degree of freedom. In the case of three electrons the correlated coordinates may be defined by

$$\begin{aligned} z_a &= \frac{1}{\sqrt{3}}[z_1 + z_2 + z_3], \\ z_b &= \frac{1}{\sqrt{6}}[2z_1 - z_2 - z_3], \\ z_c &= \frac{1}{\sqrt{2}}[z_2 - z_3]. \end{aligned} \tag{11}$$

The totally symmetric z_a coordinate describes the center-of-mass degree of freedom and the remaining z_b and z_c coordinates span the internal space [21]. It is noted that the same set of coefficients used to define the internal space, namely, $\frac{1}{\sqrt{6}}(2,-1,-1)$ and $\frac{1}{\sqrt{2}}(1,-1)$ for the z_b and z_c coordinates also appear as coefficients in the two doublet spin functions of $\left|\frac{1}{2},\frac{1}{2}\right\rangle_b$ and $\left|\frac{1}{2},\frac{1}{2}\right\rangle_a$, respectively. The internal space for the four electron case can be similarly defined. In the following the internal space for two electrons is analyzed it in detail.

The Hamiltonian (1) for quasi-one-dimensional two-electron quantum dots is simplified by neglecting the x and y degrees of freedom and by approximating the confining Gaussian potential by a harmonic-oscillator potential with ω_z

$$\mathcal{H}_{\rm 1D}^{\rm harm} = -\frac{1}{2}\frac{\partial^2}{\partial z_1^2} - \frac{1}{2}\frac{\partial^2}{\partial z_2^2} + \frac{1}{2}\omega_z^2 z_1^2 + \frac{1}{2}\omega_z^2 z_2^2 + \frac{1}{|z_1 - z_2|}. \tag{12}$$

By introducing the correlated coordinates of Eq. (10) this Hamiltonian takes the form

$$\mathcal{H}_{\rm 1D}^{\rm harm} = -\frac{1}{2}\frac{\partial^2}{\partial z_s^2} + \frac{1}{2}\omega_z^2 z_s^2 - \frac{1}{2}\frac{\partial^2}{\partial z_a^2} + \frac{1}{2}\omega_z^2 z_a^2 + \frac{1}{\sqrt{2}|z_a|}. \tag{13}$$

The first two terms on the right-hand side of Eq. (13) represent a harmonic-oscillator Hamiltonian for the z_s coordinate. They contribute the eigenenergy of a one-dimensional harmonic oscillator with frequency ω_z to the total energy. The remaining terms on the right-hand side of Eq. (13) represent a harmonic-oscillator Hamiltonian for the z_a coordinate with an additional Coulomb-type potential originating from the electron-electron interaction potential. These z_a-dependent terms account for the variation of the energy spectrum for different confinement strengths ω_z as has been observed in Fig. 2 (a). The potential energy function of these x_a-dependent terms, i.e., the sum of the harmonic-oscillator potential and the Coulomb-type potential, has been plotted in Fig. 3 for different strengths ω_z. In this figure the maximum potential height V_{max} and the domain of the z_a coordinate are $V_{max} = \omega_z \times 10$ and $|z_a| \leq \sqrt{\frac{20}{\omega_z}}$, respectively, for all ω_z. The

harmonic-oscillator part of the potential function is indicated by dotted lines in order that the role of the electron-electron interaction can be clearly seen. It appears to be identical for all ω_z values. The sharp increase at the origin of the solid line representing the diverging contribution of the electron-electron interaction potential divides the region into the two parts separated by a wall. This *potential wall* becomes stronger as ω_z decreases from (a) to (c). In case (a), corresponding to $\omega_z = 5.0$, the potential wall is rather thin and only acts as a small perturbation to the harmonic-oscillator potential. Consequently, in this case the eigenenergy of the Schrödinger equation is basically that of the harmonic-oscillator potential modified by a small energy shift. As ω_z becomes smaller the potential wall becomes thicker as displayed in Fig. 3 (b), corresponding to $\omega_z = 1.0$, and the energy shift due to the potential wall becomes larger. This observation agrees with the large splitting of the energy levels within each of the v_p manifolds as displayed in Fig. 2 (a) for the medium confinement regime.

It is noted that the eigenstates χ of the one-dimensional harmonic-oscillator with an even quantum number, χ_{even}, are affected more strongly by the potential wall than those with an odd quantum number, χ_{odd}, since the states with an even quantum number have a finite amplitude at the origin while the states with an odd quantum number have a node at the origin. Since χ_{even} and χ_{odd} are symmetric and antisymmetric with respect to the inversion of the z_a coordinate, respectively, they are symmetric and antisymmetric with respect to the interchange of electrons 1 and 2. This means that χ_{even} and χ_{odd} must be coupled to the singlet and triplet spin functions, respectively. Therefore, as ω_z decreases the triplet states become more stabilized relative to the singlet states. This effect can be clearly seen in the energy spectrum of Fig. 2 (a) where the triplet levels (colored in red) become lowered as ω_z decreases from 5.0 to 1.0.

When ω_z becomes even smaller and reaches the small confinement regime corresponding to $\omega_z = 0.1$ the potential wall becomes so thick that the wave function can hardly penetrate it. As a result the amplitude of singlet wave functions in the vicinity of the origin becomes extremely small. Therefore, except for the phase along the z_a coordinate, the nodal pattern of singlet wave functions becomes almost identical with that of the corresponding triplet wave functions having the same number of nodes as the singlet wave functions except for the node at the origin. This rationalizes the singlet-triplet doublet structure of the energy spectrum of Fig. 2 (a) for $\omega_z = 0.1$. Another nonrigorous, yet simple, explanation of the doublet structure is given by considering the average distance between the two electrons. In the limit of small confinements the relative distance between the two electrons becomes very large. Therefore the total energy does hardly depend on the mutual orientation of the electron spins implying the degeneracy of the singlet and triplet states.

Another observation that needs to be explained is the recovering of the harmonic band structure in the small ω_z regime. As the potential energy function of Fig. 3 (c) indicates, the potential wall due to the electron-electron interaction is so thick that it divides the internal space into the two regions, i.e., $z_a < 0$ and $z_a > 0$. Using the eigenfunctions χ of a particle bound in either of these two regions, χ^- and χ^+, for $z_a < 0$ and $z_a > 0$, respectively, the solution in the entire region of the potential of Fig. 3 (c) can be approximated by the sum and the difference of the functions χ^- and χ^+, respectively, because the wave function should be localized in both regions and has to satisfy the

symmetry condition. The symmetric $\frac{1}{\sqrt{2}}(\chi^- + \chi^+)$ and the antisymmetric $\frac{1}{\sqrt{2}}(\chi^- - \chi^+)$ functions describe the singlet and the triplet states, respectively, as explained earlier. On the other hand, since at $|z_a| \to \infty$ both functions $\chi^\pm$ satisfy the same boundary condition as the harmonic oscillator and vanish at the origin, the functions $\chi^\pm$ can be approximated by eigenfunctions of the harmonic oscillator with *odd* quantum numbers that have a node at the origin. Consequently, the eigenenergies associated with the symmetric and the antisymmetric solutions are given by the harmonic oscillator energies and produce a harmonic-oscillator type energy spectrum.

Finally, the number of levels in each band displayed in Fig. 2 (a) for the small ω_z regime can be rationalized by the following considerations. Since in the small ω_z regime the singlet and triplet levels always appear as degenerate doublets the pattern of the triplet states determines the number of levels. As shown in the previous paragraph the potential wall of the electron-electron interaction does not strongly affect the nodal pattern of the triplet wave functions. Therefore the polyad quantum numbers can still be used to classify the triplet levels for small ω_z. On the other hand, the singlet wave functions are affected more strongly by the potential wall for smaller ω_z and in the limit of weak confinements result in a 'node' at the origin but keep the phase of a singlet. Therefore it is convenient to extend the definition of the polyad quantum number for singlet levels by including the node at the origin. For two electrons the *extended* polyad quantum number v_p^* is defined to be identical with v_p for the triplet levels but to be $(v_p + 1)$ for the singlet levels. Using this definition the doublet pair of singlet and triplet levels has the same v_p^* value. Starting from the smallest v_p^* value of 1 for the lowest configuration of (0,1) the possible triplet configurations are (0,2) for $v_p^* = 2$, (0,3) and (1,2) for $v_p^* = 3$, and, (0,4) and (1,3) for $v_p^* = 4$. Therefore the number of levels belonging to each v_p^* manifold is calculated by using these numbers multiplied by two for a singlet and a triplet state, i.e., as 2, 2, 4, 4 for $v_p^* =$ 1, 2, 3, 4, respectively. The results agree with the number of levels displayed in Fig. 2 (a).

The case of three and four electrons is more complicated but the two characteristic features of the energy spectra observed for small ω_z, i.e., the nearly-degenerate multiplet structure of the energy levels of different spin multiplicities and the harmonic band structure of these levels, can be rationalized in a similar way. In the case of three electrons, for example, the internal space can be defined by the two correlated coordinates z_b and z_c defined by Eq. (11). The potential function becomes a sum of two harmonic-oscillator Hamiltonians for the z_b and z_c coordinates plus *three* Coulomb-type potentials originating from the three electron-electron interaction potentials $\frac{1}{|z_1 - z_2|}$, $\frac{1}{|z_2 - z_3|}$ and $\frac{1}{|z_3 - z_1|}$. As ω_z becomes smaller these three potential walls become thicker and divide the two-dimensional internal space spanned by z_b and z_c into the six regions [21]. The quartet wave functions for three electrons are not strongly affected by the potential walls since they have *nodal lines* along the three potential walls in order to satisfy the Pauli principle as in the case of triplet wave functions for two electrons. The doublet wave functions, on the other hand, have a finite amplitude along the lines of the potential walls since they do not change the sign with respect to the exchange of any two of the three electron coordinates. Therefore they are affected more strongly by the potential walls for smaller ω_z like in the case of the singlet wave functions for the two electrons. In the limit of very weak confinement they have almost no amplitude along the lines of the potential walls and their nodal pattern and energy become almost identical with those of the corresponding quartet states except

Table 3
Orbital configuration for the highest spin state of two, three and four electrons belonging to each v_p manifold.

v_p	2e	3e	4e
1	(0,1)		
2	(0,2)		
3	(0,3) (1,2)	(0,1,2)	
4	(0,4) (1,3)	(0,1,3)	
5	(0,5) (1,4) (2,3)	(0,1,4) (0,2,3)	
6		(0,1,5) (0,2,4) (1,2,3)	(0,1,2,3)
7		(0,1,6) (0,2,5) (0,3,4) (1,2,4)	(0,1,2,4)
8			(0,1,2,5) (0,1,3,4)
9			(0,1,2,6) (0,1,3,5) (0,2,3,4)
10			(0,1,2,7) (0,1,3,6) (0,1,4,5) (0,2,3,5) (1,2,3,4)

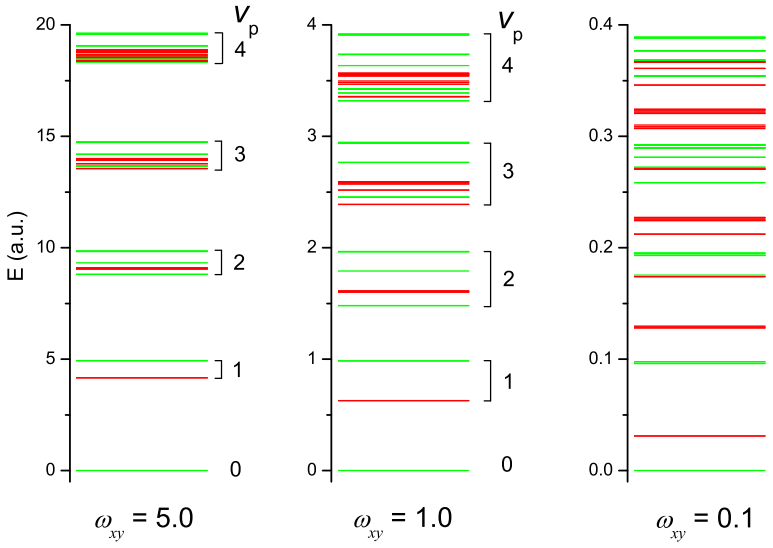

Figure 4. (Color online) Energy spectrum of the low-lying states of two electrons confined in a quasi-two-dimensional Gaussian potential for different strength of confinement. Energy levels are colored by green for singlet states and red for triplet states, respectively. The parameter v_p specifies the polyad quantum number (See the text for details).

for the phase of the wave functions. For the four electron case the situation is similar except that the internal space is three dimensional which is divided by six potential walls.

For three and four electrons the number of levels belonging to each v_p^* band in the weak confinement regime can be calculated by examining the level pattern for the highest spin states, namely, quartet and quintet, respectively. Since the spin function of the highest spin state is totally symmetric with respect to the interchange of any two electrons it can only be coupled with orbital configurations involving distinct orbitals. The orbital configurations that may be coupled to the triplet, quartet, and quintet spin states of respectively, two, three, and four electrons, are listed in Table 3 for the range of v_p^* values that appear in the energy spectra of Fig. 2. The number of levels belonging to each v_p^* manifold can be calculated from this table by counting the number of orbital configurations for each v_p^* and by multiplying this number by the factor of 2, 3, and 6 for two, three, and four electrons, respectively. In the case of four electrons the number of configurations equals to 1, 1, 2, 3, and 5 for $v_p^* = 6$, 7, 8, 9, and 10, respectively. Multiplying by the factor of 6 the number of possible levels becomes equal to 6, 6, 12, 18, and 30 for $v_p^* = 6$, 7, 8, 9, and 10, respectively. These results agree with the number of levels appearing in the energy spectrum displayed in Fig. 2 (c) for $\omega_z = 0.1$.

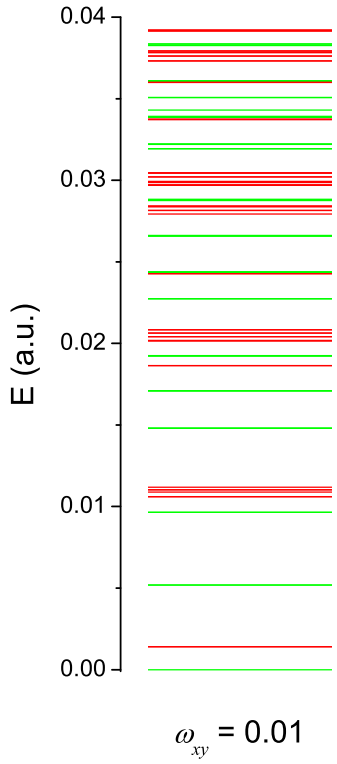

Figure 5. (Color online) Energy spectrum of the low-lying states of two electrons confined in a quasi-two-dimensional Gaussian potential for $(D, \omega_{xy}) = (0.4,\ 0.01)$. Energy levels are colored by green for singlets and by red for triplets.

4. QUASI-TWO-DIMENSIONAL QUANTUM DOTS

The energy spectrum of two electrons confined in a *quasi-two-dimensional* Gaussian potential defined by Eq. (3) is presented in Fig. 4 for different confinement strengths in a similar form as in Fig. 2 (a) for quasi-one-dimensional quantum dots. The displayed energy spectrum for the large and medium confinement regime of $\omega_{xy} = 5.0$ and 1.0 shows a polyad structure which is similar to that found for quasi-one-dimensional quantum dots shown in Fig. 2 (a) except that it involves a larger number of levels in each polyad manifold due to the increased dimensionality. For the small confinement regime of $\omega_{xy} = 0.1$, on the other hand, the energy spectrum is qualitatively different from that found in the corresponding quasi-one-dimensional case. In the first place, for quasi-two-dimensional quantum dots (cf. Fig. 4) the doublet structure consisting of a pair of singlet and triplet levels a typical feature found in the case of quasi-one-dimensional quantum dots indicating the formation of a Wigner lattice is absent. Moreover, the energy levels of a quasi-two-dimensional quantum dot with $\omega_{xy} = 0.1$ do not seem to form in the high energy region $E > 0.25$ a clearly defined band structure like in the case of quasi-one-dimensional quantum dots.

It may be argued that the energy spectrum in the smal confinement regime correspond-

ing to $\omega_{xy} = 0.1$ displayed in Fig. 4 shows a tendency to form a Wigner lattice for even smaller values of ω_{xy}. In order to check this a quasi-one-dimensional quantum dot for confinement strength as small as $\omega_{xy} = 0.01$ has been studied. The resulting energy spectrum is presented in Fig. 5. Again, the displayed spectrum shows no singlet-triplet doublet structure. Quite to the contrary, it becomes more difficult to recognize a band structure in the spectrum. Thus, the energy spectrum of quasi-two-dimensional quantum dots in the weak confinement regime seems to be essentially different from that of quasi-one-dimensional quantum dots.

In order to analyze the origin of this difference between the energy spectra of quasi one- and two-dimensional quantum dots in the small confinement regime the internal space for two electrons is considered like in the quasi-one-dimensional cases. Using a harmonic approximation to the Gaussian confining potential and neglecting the dependence on the z coordinate the Hamiltonian of Eq. (1) for two electrons takes the form

$$\begin{aligned}\mathcal{H}_{\rm 2D}^{\rm harm} &= -\frac{1}{2}\left[\frac{\partial^2}{\partial x_1^2}+\frac{\partial^2}{\partial y_1^2}\right]-\frac{1}{2}\left[\frac{\partial^2}{\partial x_2^2}+\frac{\partial^2}{\partial y_2^2}\right]+\frac{1}{2}\omega_{xy}^2\left[x_1^2+y_1^2\right]+\frac{1}{2}\omega_{xy}^2\left[x_2^2+y_2^2\right]\\ &\quad+\frac{1}{\sqrt{(x_1-x_2)^2+(y_1-y_2)^2}}.\end{aligned} \tag{14}$$

Performing the unitary transformation of the independent electron coordinates (x_1,y_1,x_2,y_2) into the correlated coordinates (x_s,y_s,x_a,y_a),

$$\begin{aligned}x_s &= \frac{1}{\sqrt{2}}[x_1+x_2],\\ y_s &= \frac{1}{\sqrt{2}}[y_1+y_2],\\ x_a &= \frac{1}{\sqrt{2}}[x_1-x_2],\\ y_a &= \frac{1}{\sqrt{2}}[y_1-y_2],\end{aligned} \tag{15}$$

the Hamiltonian of Eq. (14) separates into a sum of two contributions, depending either on the coordinates (x_s, y_s) or (x_a, y_a), i.e.,

$$\mathcal{H}_{\rm 2D}^{\rm harm} = \mathcal{H}_{\rm c.o.m}(x_s, y_s) + \mathcal{H}_{\rm int}(x_a, y_a), \tag{16}$$

where

$$\mathcal{H}_{\rm c.o.m} = -\frac{1}{2}\left[\frac{\partial^2}{\partial x_s^2}+\frac{\partial^2}{\partial y_s^2}\right]+\frac{1}{2}\omega_{xy}^2\left[x_s^2+y_s^2\right], \tag{17}$$

and

$$\mathcal{H}_{\rm int} = -\frac{1}{2}\left[\frac{\partial^2}{\partial x_a^2}+\frac{\partial^2}{\partial y_a^2}\right]+\frac{1}{2}\omega_{xy}^2\left[x_a^2+y_a^2\right]+\frac{1}{\sqrt{2(x_a^2+y_a^2)}}. \tag{18}$$

The first part of the Hamiltonian (16), $\mathcal{H}_{\rm c.o.m}$, describes the center-of-mass contribution as in the quasi-one-dimensional cases and contributes the eigenenergy of a two-dimensional

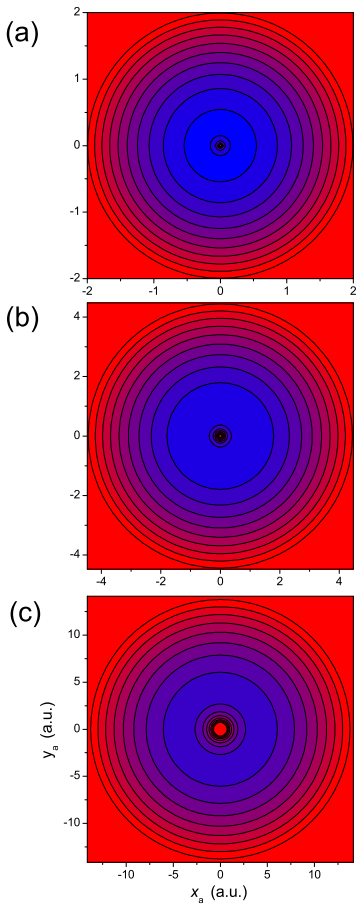

Figure 6. (Color online) Two-dimensional contour plot of the sum of the harmonic-oscillator and of the electron-repulsion potentials for two electrons in the internal space (x_a, y_a) for $\omega_{xy} = 5.0$ (a), 1.0 (b), and 0.1 (c). The maximum potential height V_{max} and the domain of the x_a and y_a coordinates displayed are the same as used in Fig. 3. The red spot at the origin of the contours represents the *potential pole* of the electron repulsion potential.

isotropic harmonic oscillator to the total energy. The second part of the Hamiltonian, $\mathcal{H}_{\rm int}$, depends on the antisymmetric coordinates x_a and y_a and represents the contribution to the total energy due to the internal degrees of freedom.

In order to explain the characteristic feature of the energy spectrum that distinguishes it from the quasi-one-dimensional case the potential energy function has been plotted for the internal Hamiltonian of Eq. (18) for different ω_{xy} values in Fig. 6. The maximum height of the potential V_{max} and the domain of the x_a and y_a coordinates are the same as for the quasi-one-dimensional potential presented in Fig. 3. Implying that the harmonic-oscillator part of the potential looks identical for different ω_{xy} values the effect of the electron-electron interaction becomes apparent. The small red spot at the center of the potential represents a sharp increase due to the electron-electron interaction. It increases in size as ω_{xy} becomes smaller. This indicates that the electron-electron interaction perturbs the harmonic-oscillator potential more strongly for smaller confinement like in the quasi-one-dimensional case. It is noted, however, that the potential energy function has a pole rather than a potential wall like in the quasi-one-dimensional case where the wall separates the internal space into two regions. As a consequence, the electron-electron interaction potential in the quasi-two-dimensional case will not strongly modify the nodal pattern of singlet wave functions since they can avoid the pole. Therefore there seems to be little reason for the singlet and triplet levels of quasi-two-dimensional quantum dots to form in the weak confinement regime degenerate pairs unlike in the case of quasi-one-dimensional quantum dots.

5. SUMMARY

In the present study the energy-level structure of two, three and four electrons confined in a quasi-one-dimensional Gaussian potential for different strength of confinement has been examined in detail by using the accurate computational results of eigenenergies and wave functions obtained in previous studies for two and three electrons and in the present study for four electrons, respectively. The eigenenergies and wave functions have been calculated by using the quantum chemical full configuration interaction method and by employing Cartesian anisotropic Gaussian basis sets with high angular momentum functions. The energy-level structure changes qualitatively for different strength of confinement and is classified by three regimes of the strength of confinement ω_z, namely, large, medium and small. The polyad quantum number v_p has been used to characterize the energy-level structure for large and medium ω_z while the *extended* polyad quantum number v_p^* has been used for small ω_z. The energy levels at the small ω_z regime form nearly-degenerate multiplets consisting of a set of energy levels having different spin multiplicities. To analyze the effect of the electron-electron interaction on the formation of the degenerate multiplets the *potential energy function* defined by the sum of the one-electron potentials and the two-electron potentials has been introduced and displayed as function of the internal space for different strengths of ω_z. The plots of the potential energy function for different ω_z clearly show that for small ω_z the degeneracy of the energy levels among different spin states is caused by the *potential walls* of the electron-electron interaction potentials within the internal space. A systematic way of obtaining the degeneracy pattern of energy levels for small ω_z is given.

The energy spectrum of two electrons confined in a quasi-*two*-dimensional Gaussian potential has also been studied for the same set of the strengths of confinement as the corresponding quasi-one-dimensional cases and are compared to them. The energy spectrum of the quasi-two-dimensional quantum dot is qualitatively different from that of the quasi-one-dimensional quantum dot in the small confinement regime. The origin of the differences is due to the difference in the structure of the internal space.

REFERENCES

1. C. B. Murray, D. J. Norris and M. G. Bawendi, J. Am. Chem. Soc. 115 (1993) 8706.
2. R. C. Ashoori, Nature 379 (1996) 413.
3. S. Tarucha, D. G. Austing, T. Honda, R. T. van der Hage and L. P. Kouwenhoven, Phys. Rev. Lett. 77 (1996) 3613.
4. N. F. Johnson, J. Phys.: Condens. Matter 7 (1995) 965.
5. L.P. Kouwenhoven, T. H. Oosterkamp, M. W. S. Danoesastro, M. Eto, D. G. Austing, T. Honda and S. Tarucha, Science 278 (1997) 1788.
6. P. Matagne, J. P. Leburton, D. G. Austing and S. Tarucha, Physica E 13 (2002) 679.
7. A. P. Alivisatos, Science 271 (1996) 933.
8. T. Ezaki, N. Mori and C. Hamaguchi, Phys. Rev. B 56 (1997) 6428.
9. G. Cantele, D. Ninno and G. Iadonisi, Phys. Rev. B 64 (2001) 125325.
10. B. Szafran, J. Adamowski and S. Bednarek, Physica E 5 (2000) 185.
11. T. Sako, S. Yamamoto and G. H. F. Diercksen, J. Phys. B: At. Mol. Opt. Phys. 37 (2004) 1673.
12. U. Merkt, J. Huser and M. Wagner, Phys. Rev. B 43 (1991) 7320.
13. P. A. Maksym and T. Chakraborty, Phys. Rev. Lett. 65 (1990) 108.
14. J. Hu, T. W. Odom and C. M. Lieber, Acc. Chem. Res. 32 (1999) 435.
15. M. Rontani, F. Rossi, F. Manghi and E. Molinari, Phys. Rev. B 59 (1999) 10165.
16. T. Sako and G. H. F. Diercksen, J. Phys. B: At. Mol. Opt. Phys. 36 (2003) 1433.
17. T. Sako and G. H. F. Diercksen, J. Phys.: Condens. Matter 15 (2003) 5487.
18. T. Sako and G. H. F. Diercksen, J. Phys.: Condens. Matter 17 (2005) 5159.
19. T. Sako, P. A. Hervieux and G. H. F. Diercksen, Phys. Rev. B 74 (2006) 045329.
20. T. Sako and G. H. F. Diercksen, Phys. Rev. B 75 (2007) 115413.
21. T. Sako and G. H. D. Diercksen, J. Phys.: Condens. Matt. 20 (2008) 155202.
22. T. Sako and G. H. F. Diercksen, J. Phys. B: At. Mol. Opt. Phys. 36 (2003) 1681.
23. P. Matagne and J. P. Leburton, Phys. Rev. B 65 (2002) 235323.
24. J. Adamowski, M. Sobkowicz, B. Szafran and S. Bednarek, Phys. Rev. B 62 (2000) 4234.
25. M. Wagner, U. Merkt, A. V. Chaplik, Phys. Rev. B 45 (1992) 1951.
26. J. T. Lin and T. F. Jiang, Phys. Rev. B 64 (2001) 195323.
27. O. Dippel, P. Schmelcher and L. S. Cederbaum, Phys. Rev. A 49 (1994) 4415.
28. W. Becken, P. Schmelcher and F. K. Diakonos, J. Phys. B: At. Mol. Opt. Phys. 32 (1999) 1557.
29. P. S. Drouvelis, P. Schmelcher and F. K. Diakonos, J. Phys.: Condens. Matter 16 (2004) 3633.
30. P. S. Drouvelis, P. Schmelcher and F. K. Diakonos, Phys. Rev. B 69 (2004) 035333.

31. M. Braskén, M. Lindberg, D. Sundholm and J. Olsen, Phys. Rev. B 61 (2000) 7652.
32. S. Corni, M. Braskén, M. Lindberg, J. Olsen and D. Sundholm, Phys. Rev. B 67 (2003) 085314.
33. G. W. Bryant, Phys. Rev. Lett. 59 (1987) 1140.
34. W. Duch and J. Karwowski, Comput. Phys. Rep. 2 (1985) 93.
35. M. Kotani, A. Amemiya, E. Ishiguro and T. Kimura, Table of Molecular Integrals (Tokyo: Maruzen) (1995).
36. B. Szafran, F. M. Peeters, S. Bednarek, T. Chwiej and J. Adamowski, Phys. Rev. B 70 (2004) 035401.
37. E. Wigner, Phys. Rev. 46 (1934) 1002.